Article

Cage Encapsulated Gold Nanoparticles as Heterogeneous Photocatalyst for Facile and Selective Reduction of Nitroarenes to Azo compounds

Bijnaneswar Mondal, and Partha Sarathi Mukherjee

J. Am. Chem. Soc., **Just Accepted Manuscript** • DOI: 10.1021/jacs.8b07767 • Publication Date (Web): 10 Sep 2018

Cage Encapsulated Gold Nanoparticles as Heterogeneous Photocatalyst for Facile and Selective Reduction of Nitroarenes to Azo compounds

Bijnaneswar Mondal and Partha Sarathi Mukherjee*

Department of Inorganic and Physical Chemistry, Indian Institute of Science, Bangalore 560012, India.

Supporting Information

ABSTRACT: A discrete nanoscopic organic cage (**OC1^R**) has been synthesized from a phenothiazine based trialdehyde treating with chiral 1,2-cyclohexanediamine building block via dynamic imine bond formation followed by reductive amination. The cage compound has been characterized by several spectroscopic methods which advocate that **OC1^R** has trigonal prismatic shape formed via [2+3] self-assembled imine condensation followed by imine reduction. This newly designed cage has aromatic walls and porous interior decorated with two cyclic thioether and three vicinal diamine moieties suitable for binding gold ions to engineer the controlled nucleation and stabilization of ultrafine gold nanoparticles (AuNPs). The functionalized confined pocket of the cage has been used for the controlled synthesis of AuNPs with narrow size distribution via encapsulation of Au(III) ions. Inductively coupled plasma mass spectrometric (ICP-MS) analysis revealed that the composite **Au@OC1^R** has very high (~68 wt%) gold loading. In distinction, reduction of gold salts in absence of the cage yielded structure less agglomerates. The fine-dispersed cage anchored AuNPs (**Au@OC1^R**) have been finally used as potential heterogeneous photocatalyst for very facile and selective conversion of nitroarenes to respective azo compounds at ambient temperature in just 2 h reaction time. Exceptional chemical stability and reusability without any agglomeration of AuNPs even after several cycles of use are the potential features of this material. The composite **Au@OC1^R** represents the first example of organic cage supported gold nanoparticles as photocatalyst.

INTRODUCTION

Heterogeneous photocatalysts[1] seize a great attention in the past decade over conventional catalysts in terms of converting solar energy into clean hydrogen energy by splitting water, and decomposing harmful organic/inorganic pollutants. Semiconductors based gold nanoparticles[2] (AuNPs) such as Au/TiO_2 were extensively used in various organic transformations as photocatalysts in green chemistry approach. It is well-known that AuNPs are chemically very stable in nano-levels with exceptional properties such as the localised surface plasmon resonance (LSPR) effect.[3] LSPR denotes as a collective oscillation of conduction-band (CB) electrons which are in resonance with the oscillating electromagnetic field of incident light. The decay of excited LSPR can produce hot electrons and holes at the proximity of AuNPs surfaces to initiate chemical reactions.[4] Moreover, AuNPs exhibit strong ultraviolet (UV) absorption that leads to an interband excitation of electrons from 5d to 6sp.[5] The photoexcitation of such AuNPs can be used to endorse electron transfer that would not be thermodynamically feasible in the ground electronic state.[6] Therefore, such kind of process can produce unstable intermediates under mild conditions[7] that would have been forbidden in a thermal reaction at high pressure. It is established that AuNPs size and surface properties of the support are pivotal in determining photocatalytic activity widely.[8] However, our present work demonstrates the first time use of a discrete organic cage supported AuNPs as very efficient photocatalyst in organic transformation.

In recent times by articulating different organic spacers with suitable metal centers, many shape-persistent discrete assemblies have been developed.[9,10] Furthermore, dynamic covalent chemistry[11] has emerged as an effective approach for the easy construction of organic architectures having shapes and sizes analogous to coordination assemblies. To this end, well-defined pore structures of such materials have been exploited as template to synthesize metal nano-particles (MNPs) of different shapes and sizes. Compared to bulk metal counterparts, MNPs having high surface-to-volume ratio with many active catalytic sites per unit area make them better candidates for superior catalytic performance.[12] But such tiny MNPs having high surface energy leads to the formation of aggregates during reactions leading to poor catalytic activity.[13f] To overcome this problem, several supports like metal oxides,[14] metal-organic frameworks,[15] dendrimers,[13] covalent organic frameworks[16] have been used in last few years. Despite of considerable advancement in this area, development of new templates for accurate control over the size distribution and stability of the MNPs is still a great challenge. To address the above-mentioned issues, discrete organic cages have attracted tremendous attention owing to their structural tunability and chemical/thermal stability for homogeneous/heterogeneous catalysis.[17]

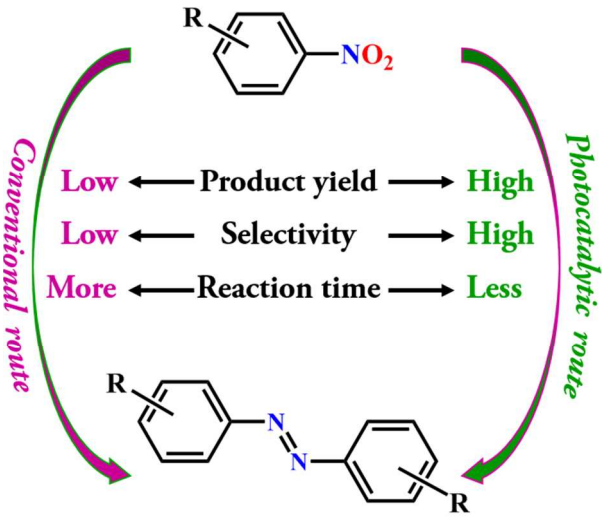

Figure 1. Schematic representation of conventional azo synthesis and photocatalytic routes for azo synthesis using **Au@OC1^R** as photocatalyst.

Aromatic azo compounds have diverse applications in academic and industrial research, such as in organic dyes,[18] food additives,[19] pigments,[20a] colorants,[20c] therapeutic agents,[20b,d] and as precursors of natural products synthesis.[21] Conventional approaches for the development of aromatic azo compounds involve the use of stoichiometric amounts of nitrite salts ($NaNO_2$) or toxic oxidants via diazonium salts [22] or nitroso-benzene intermediates.[23] Several catalytic protocols have been developed recently for the synthesis of azo derivatives but the existing approaches[24] have numerous drawbacks, like tedious work-up process, lower yields, undesirable toxic side products, poor catalyst reusability, limited functional-group compatibility with poor selectivity (Figure 1). Formation of azoxy, amine derivatives and other byproducts is the common drawback in the synthesis of azo compounds using traditional approach. Thus, finding a more gentle and economical heterogeneous protocol which is more concise, more versatile and more chemo-selective for the reduction of nitroarenes under mild conditions is highly desirable.

Herein, we report the size controlled synthesis of AuNPs of very narrow size distribution (~ 2 nm) using a multifunctionalized nanoscopic organic cage as template. Large confined pocket with interior decoration employing cyclic thioether/vicinal diamine helped nucleation and stabilization of gold nanoparticles with controlled size distribution. Furthermore, such cage anchored AuNPs have been utilized as heterogeneous photocatalyst for very selective and facile conversion of nitroarenes to corresponding azo-compounds at ambient temperature in very high yield in just 2 h reaction time. The newly developed composite **Au@OC1^R** represents the first example of cage supported gold nanoparticles used as photocatalyst.

RESULTS AND DISCUSSIONS

Synthesis and Characterization of the Organic Cage: Molecular trigonal-prismatic cage **OC1^R** was synthesized (~ 83% yield) via the reaction of phenothiazine based trialdehyde **P3** with a chiral diamine **4** [(S, S)-1, 2-cyclohexanediamine] (Scheme 1). The trialdehyde building block **P3** was synthesized by a multistep synthetic procedure starting from phenothiazine (Scheme S1). By treating trialdehyde **P3** with diamine **4** in 2:3 stoichiometric ratio in chloroform at room temperature for 48 h yielded imine based organic cage **OC1** which was isolated as a yellow powder. Molecular cage with [2 + 3] assembly of the aldehyde and amine is enthalpically favored owing to the least angle strain; and entropically favored as it comprises of minimum number of building blocks compared to all the possible 3D architectures.[11b] Imine bonds are sensitive to water and strong acids/bases. Hence, the imine cage (**OC1**) was converted to stable amine cage **OC1^R** by treating with sodium borohydride which reduced the imine bonds. As synthesized **OC1^R** was well characterized by multinuclear NMR (^{1}H, ^{13}C), ^{1}H-^{1}H COSY, ^{1}H NOESY, ^{1}H DOSY, FT-IR and ESI-MS analyses (Figures S18-S23). The formation of [2+3] assembled molecular cage was unambiguously established by the peak at m/z = 1269.6366 corresponding to $[M+H]^+$ in ESI-MS spectrum (Figure S21).

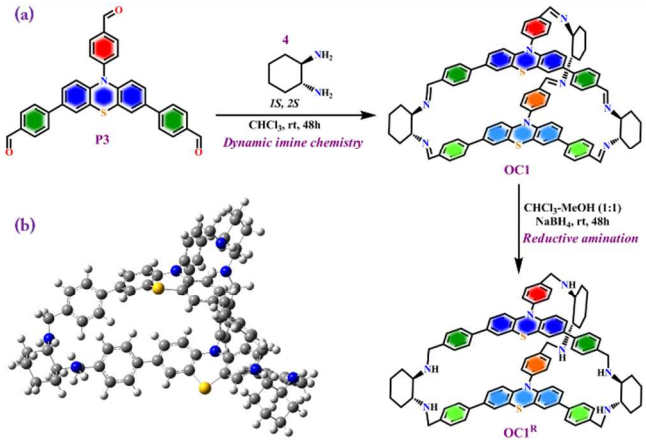

Scheme 1. (a) Synthetic Routes for the Synthesis of Molecular Trigonal Prism **OC1^R**, (b) Gas-Phase DFT (B3LYP/6-31G)-Optimized Structure of the Organic Cage **OC1^R**.

Numerous efforts of crystallization of **OC1^R** have so far been unsuccessful. Yet, gas phase DFT (B3LYP/6-31G) calculation exposes that top and bottom trigonal faces of the cage are in eclipse conformation with slight parallel shift in lowest energy conformer of **OC1^R**. The distance between the sulphur atoms of the phenothiazine cores is ~ 0.94 nm while the distance between the two utmost points inside the cage is ~ 1.67 nm with an outer distance of ~2.31 nm (Figure S24).

Synthesis of Cage Infused Gold Nanoparticles (AuNPs): The cage **OC1^R** having two cyclic thioether moieties along with three vicinal diamine clefts in its backbone make it a suitable candidate for the complexa-

tion with gold(III) salts. Consequently, it is expected that two thioether and two chelating diamine moieties will strongly interact with Au^{3+} ions[17] and promote the controlled nucleation of AuNPs along with the stabilization by the furnished aromatic backbones. We also anticipated that the cage template can offer a protecting shell with least coverage and superior AuNPs surface accessibility due to the presence of large open-windows of the cage.

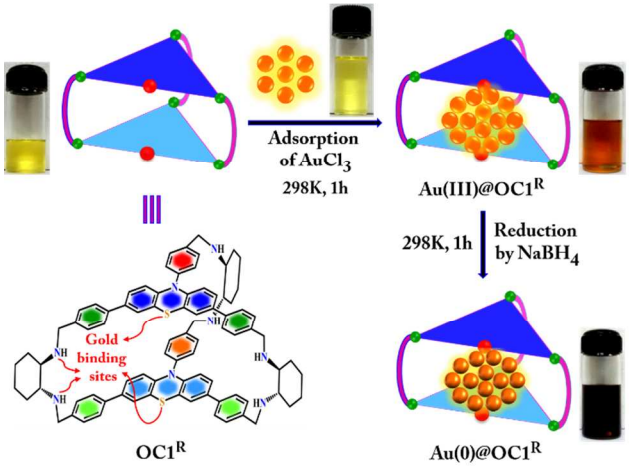

Figure 2. Schematic illustration of two-step formation of **Au@OC1^R** (inset images are shown for different materials).

Treating one equivalent of **OC1^R** with fourteen equivalents of $AuCl_3$ showed a sharp color change from yellow to brown at room temperature (Figure 2) due to the binding of gold ions with the cage compound as confirmed by ^{1}H, ^{1}H 2D NMR and XPS (Figures S27, S30-S32). Subsequently, a methanolic solution of four equivalents sodium borohydride was added to this reaction mixture and immediately brown solution was turned into black without any precipitation. This result indicates reduction of Au^{3+} ions into Au^0. After centrifugation of the resulting mixture and washing with methanol/THF, the **Au@OC1^R** was obtained as a black powder (Figure S29). Remarkably, this material was insoluble in common organic solvents except in $CHCl_3$ without any agglomeration even after several months. Experiments with lower equivalents of $AuCl_3$ with respect to the cage yielded similar AuNPs size (Figure S37) but with less gold loading. Moreover, beyond fourteen equivalents of $AuCl_3$ yielded structureless agglomerates as confirmed by TEM (Figure S38). So, 1:14 is the optimum **OC1^R**:$AuCl_3$ ratio for obtaining minimum size tiny AuNPs (~2 nm) with maximum loading (~68 wt%) of gold.

Powder X-ray diffraction (PXRD) analysis of as-synthesized **Au@OC1^R** displayed peaks at 2θ ≈ 38.3º, 44.5º, 64.7º, 77.6º and 81.8º along with peaks for **OC1^R**. These peaks could be attributed to (111), (200), (220), (311) and (222) lattice planes which are characteristic signatures for Au with a face centered cubic (fcc) structure (Figure S33). Furthermore, X-ray photoelectron spectroscopy (XPS) advocates that Au is in zero oxidation state as designated by its characteristic binding energy values of 87.7 eV and 84.0 eV corresponding to two distinct spin-orbit pairs $4f_{5/2}$ and $4f_{7/2}$, respectively (Figure 3c).

Bright field transmission electron microscopy (BF-TEM) of **Au@OC1^R** portrays the homogeneously dispersed tiny AuNPs with a narrow size distribution, having mean particle size of 1.99 ± 0.18 nm (Figures 3a and 3b). Further calculation based on the optimized structure of **OC1^R** illustrates that the estimated internal cavity size is between 1.67 to 1.82 nm. This result is in close agreement with most of the AuNPs are anchored within the organic cage (Figure S24, for more details see the Supporting Information). To validate that the AuNPs were anchored inside the cage cavity and to exclude the possibility of AuNPs bound by multiple cages in their intermolecular space, ^{1}H diffusion-ordered spectroscopy (DOSY) NMR was performed on both free cage **OC1^R** and **Au@OC1^R** at the same temperature in $CDCl_3$[17a] (Figures S26 and S28). As anticipated, we found similar diffusion coefficient values for **OC1^R** and **Au@OC1^R**, -9.78±0.01 and -9.80±0.02 respectively, which indicate the comparable size and shape of free cage **OC1^R** and **Au@OC1^R**. These results echo that the AuNPs formation is an outcome of a single cage encapsulation instead of inter-cage interactions. In the ^{1}H NMR spectrum of the **Au@OC1^R** complex, a significant broadening and shifting of not only the protons of alkyl chains (-CH_2/-CH) but also all aromatic protons of the cage structure were observed (Figure S30). This suggests that the AuNPs are wrapped by the cage skeleton and the skeletal protons experience restricted mobility with fast spin relaxation[12e,17a, d] which leads to line broadening in ^{1}H NMR spectrum. Similar kind of MNPs encapsulated organic cage was also reported by Zhang and co-workers previously.[17a]

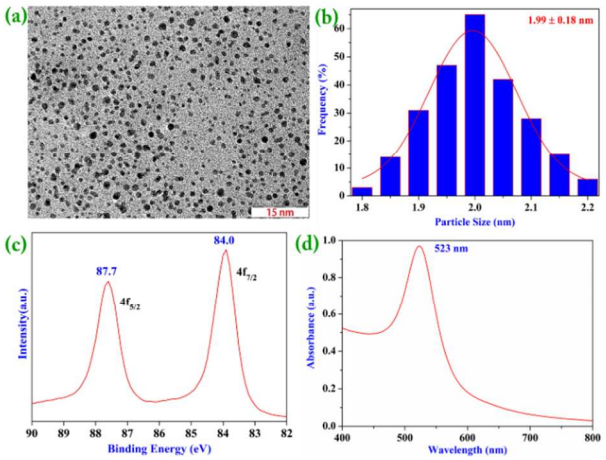

Figure 3. (a) TEM, (b) particle size distribution, (c) XPS spectrum and (d) absorption spectrum of **Au@OC1^R**.

The scanning electron microscopy (SEM) image portrays an uneven morphology (Figure S34a) composed of granular size particles of the material. Energy-dispersive X-ray spectroscopic (EDS) image of **Au@OC1^R** displayed (Figure S35) the presence Au along with other organic cage elements (C, H, N, S). The elemental mapping (Figure S34b) revealed the well dispersed nature of AuNPs at the surface during SEM experiments. The absorption peak at nearly

523 nm in the UV/Vis spectrum (Figure 3d) of the **Au@OC1^R** can be ascribed to a SPR absorption [3e,7a] by the AuNPs. Finally, the gold loading estimated by inductively coupled plasma mass spectrometry (ICP-MS) was found to be ~ 68 wt %, which is highest gold loading achieved in any porous organic cage compound till date. Typically, by the wet chemical approach beyond 20 wt% of NPs loading leads to agglomeration of metal nanoparticles (MNPs) as conveyed in preceding document.[15f]

To recognize the role of structural features (size and shape) of organic cages on the evolution of nanoparticles and their size control, we performed a controlled experiment. In that instance $AuCl_3$ in methanol was treated with four equivalents of methanolic $NaBH_4$ but in the absence of cage compound (**OC1^R**). TEM analysis of the resulting black precipitate (usually named as gold bulk i.e. **Au@bulk**) displayed the formation of structure-less bumpy agglomerates (Figure S36a). Such observation is indisputably due to the absence of nucleation sites (i.e., thio-/diamine- moieties) and confined pocket of cage for stabilization and controlling size. Similar agglomerates formation was observed when only phenothazine was used instead of cage (Figure S36b). Such a marked difference in the AuNPs size/morphology in presence and absence of cage indicates the sheer role of structural features of the organic cage on the nucleation of AuNPs including their size tuning and stabilization.

Reduction of Nitroarenes: An industry-friendly development towards one-step nitro- to azo- conversion has fundamental as well as practical interest in organic synthesis.[25] In 2008, Corma and co-workers reported that aromatic azo compounds could be synthesized from the corresponding nitroarenes through a two-step, one-pot reaction with catalysts embracing AuNPs on TiO_2 or CeO_2 at 100°C or higher.[26] In this thermal hydrogenation, azobenzene was formed as an intermediate but, it was unstable under such reaction conditions (high pressure, high temperature) and rapidly reduced to aniline.[27] As photocatalytic reactions are typically conducted at ambient temperature and atmospheric pressure,[28] several intermediates are moderately stable under such conditions. Hence, by using a photocatalytic process, the synthesis of aromatic azo compounds would be a much more simple, controlled, and greener process.

To evaluate the catalytic activity of the cage supported gold nanoparticles (**Au@OC1^R**) as photocatalyst, the reduction of 1-chloro-4-nitrobenzene has been selected as the model reaction. The reaction conditions were optimized by examining the influence/impact of catalyst loading, time and solvent in a series of experiments and the results are depicted in Table 1. The best result was obtained with 0.5 mol% of **Au@OC1^R** in 2-propanol (heterogeneous way) under UV radiation for 2 h in inert atmosphere which gave selectively corresponding azo compound with >99% conversion (Table 1, entry 4) (Figure S41, S45). A profound effect was observed on the conversion of the desired product by altering reaction parameters (Table 1, entries 1-3).

As it is already reported in literature that 2-propanol is a hydrogen donor source[7a, 14e] as well as solvent, we have tested other alcohols for checking their capability as a hydrogen donor without changing other parameters. The experimental results convey that none of solvents could deliver azo compound completely (Table 1, entries 6-8) (Figure S42). Also, no azo- formation was observed when the same reaction was performed either in absence of AuNPs or in presence of only cage **OC1^R** under identical conditions (entries 9, 11). Moreover, phenothiazine was used as catalyst which is known as a photosensitizer in the literature. But negligible amount (<1%) of azo formation was observed under both UV and visible light (entry 13) (Figure S44). It was thus evident that the reaction was driven by AuNPs; and the free cage has no catalytic role other than stabilizing the AuNPs (Figure S43).

It is well-known that the catalytic activity of NPs significantly depends on their size whereas increase in the size leads to decrease in catalytic activity. The same logic was applicable when the model reaction was done in presence of **Au@bulk** under identical reaction conditions (Table 1, entry 10). Fascinatingly, the photocatalytic reduction of model system was highly influenced by UV/visible light probably due to inter-band excitation of electrons (5d to 6sp)/ LSPR effect whereas only negligible amount (1%) of azo product was detected in dark in presence of AuNPs under identical reaction conditions (Table 1, entry 12) (Figure S43).

Table 1. Optimization of reaction parameters for the reduction of 1-chloro-4-nitrobenzene[a]

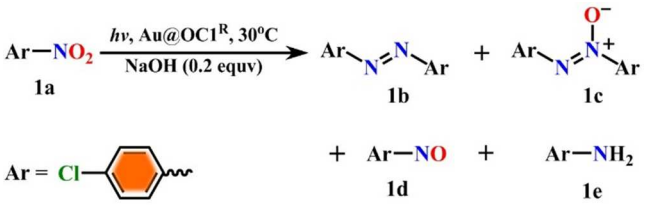

entry	solvent	time (mins)	mol% Au	conversion[b] (**1b**) [%]	
				UV	Vis
1	2-propanol	60	0.25	32	15
2	2-propanol	60	0.5	60	29
3	2-propanol	120	0.25	68	31
4	**2-propanol**	**120**	0.5	**>99**	**40**
5	2-propanol	150	0.5	>99	40
6	n-propanol	120	0.5	30	11
7	n-butanol	120	0.5	17	6
8	ethanol	120	0.5	12	1

9	2-propanol	120	0	0	0
10	2-propanol	120	0.5[c]	9	4
11	2-propanol	120	0.5[d]	0	0
12	2-propanol	120	0.5[e]	1	-
13	2-propanol	120	0.5[f]	<1	<1

[a]Reaction conditions: under N2 atmosphere in heterogeneous way, 1-chloro-4-nitrobenzene (6.35 mmol), NaOH (1.27 mmol). [b]Conversions are based on ^{1}H NMR analysis of the crude product. [c]using **Au@bulk** as catalyst. [d]using free cage **OC1^R** as catalyst. [e]using **Au@OC1^R** as catalyst in dark conditions. [f]using phenothiazine as catalyst.

To validate the general applicability of this novel heterogeneous catalyst and the scope of the procedure, we extended our synthetic strategy for a wide range of nitroarenes to produce their corresponding azo-compounds (Table 2). We were delighted to find that a numerous functionalized nitroarenes, specially electron-deficient substrates, are converted smoothly and selectively into the desired products with good to excellent yields (Table 2, entries 1–6, 13-15). Also, the electron-donating such as methyl-substituted nitrobenzenes and methoxy-substituted nitrobenzene were fully converted to the corresponding azo compounds in good yields (Table 2, entries 7–11).

It is notable that halogenated nitroarenes employed in this catalysis model lead to the formation of corresponding fluoro-, chloro-, bromo- or iodo- azo compounds without any dehalogenation (Table 2, entries 1–6). By the other procedures[24e] of azo-compounds synthesis from nitro-compounds, byproducts formation including catalytic hydrogenation is a common problem. In addition to halogen substituents, delicate reducible functional groups like ketone, nitrile, and even ester moieties were finely tolerated without undergoing reduction to any substantial extent during the photocatalytic reduction of nitro-compounds to corresponding azo-derivatives (Table 2, entries 13–15) using our newly developed **Au@OC1^R**.

Table 2. Au@OC1^R catalyzed selective reduction of various nitroarenes[a]

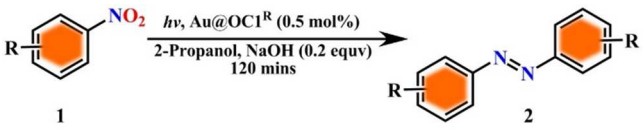

entry	product	yield[b] [%]	TOF[c] [h^{-1}]
1	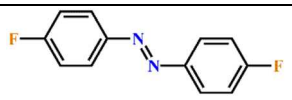	91	9100
2	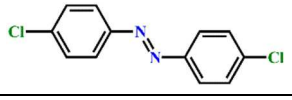	94	9400
3	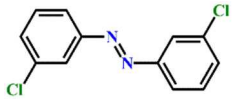	92	9200
4		89	8900
5	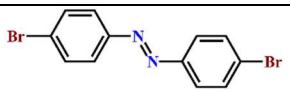	93	9300
6	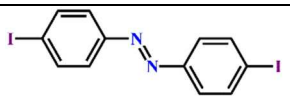	90	9000
7	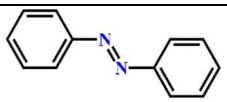	92	9200
8	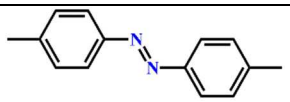	91	9100
9	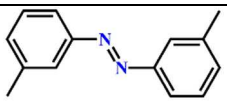	88	8800
10	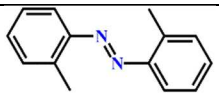	85	8500
11	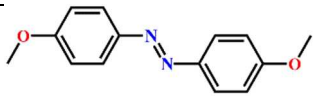	90	9000
12	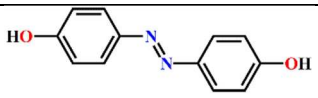	87	8700
13	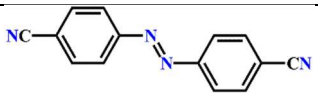	88	8800
14	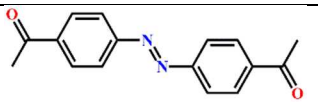	87	8700
15	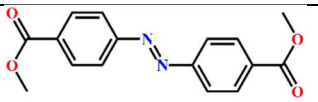	84	8400
16	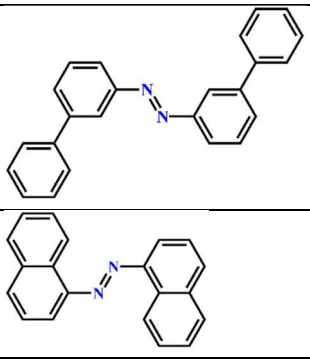	83	8300
17		80	8000

[a]Reaction conditions: under N2 atmosphere in heterogeneous way, Nitroarenes (1 equv.), NaOH (0.2 equv.), **Au@OC1^R** (0.5 mol% Au), 15 mL 2-Propanol, time 120 mins, temperature 30^{o}C. [b]Isolated yield of pure products after col-

umn chromatography. [c]Turn over frequency calculated based on isolated yield of pure product.

AuNPs have been widely used as catalyst in the reduction of 4-nitrophenl to 4-aminophenol.[16e] Such reduction of nitroarenes to amines is quite straightforward. However, using the new catalyst **Au@OC1^{R}**, we have successfully isolated its corresponding azo compound in good yield without any degradation due its sensitive -OH groups (Table 2, entry 12). Furthermore, this catalytic system has great potential to alter other polyaromatic nitroarenes like biphenyl and naphthyl to corresponding azo-derivatives with high yield, which is usually hard to achieve using traditional organic synthesis (Table 2, entries 16–17). These experimental results establish the versatility of the current methodology for selective and very facile synthesis of azo compounds with high yields.

Steric properties of the substituents also affect the reductive coupling significantly. In this fact, the substitution on phenyl ring on different positions i.e. *ortho*, *meta* and *para* was also explored in this catalytic reaction. Role of both the electron withdrawing (-Cl) as well as electron donating (-Me) groups was investigated to check the catalytic performance (Table 2, entries 2–4, 8–10). In both the cases selectivity and yields were in the order of *para*>*meta*>*ortho*. We believe these results were solely due the steric effect on phenyl ring around the AuNPs surface which always favors the para- substituent with higher yield rather than its ortho- substituent.

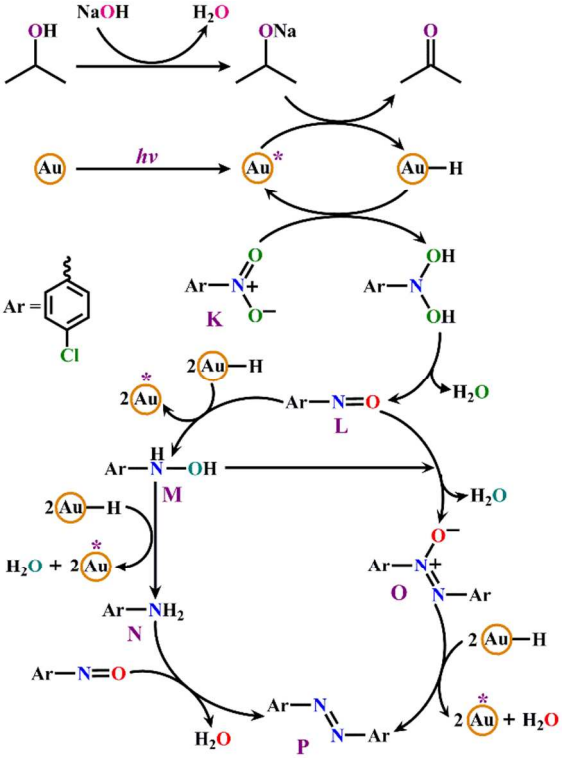

Figure 4. A plausible reaction pathway for the reduction of nitroarene in this photocatalytic process.

Although the exact routes by which the reduction occurs are not yet fully understood but based on the time dependent ^{1}H NMR and ESI-HRMS (Figures S48, S49) analysis of the reaction, we propose the following reaction steps that are involved in this photocatalytic process (Figure 4). Frist, NaOH enhances the abstraction of a hydrogen atom from 2-propanol[7a,14e] leading to the formation of sodium isopropoxide. Now, in presence of UV/Vis light, AuNPs generate hot electrons and holes at surfaces which further generate AuNPs-H species by abstracting hydride from sodium isopropoxide and leaving acetone as oxidized product. This Au—H bond is relatively stable at the AuNPs surface[12f] which transfers hydride to nitroarene (**K**) and regenerate the catalyst. Further, two hydrides transfer leads to the formation of nitroso-arene (**L**) by eliminating water. The nitroso-arene is the key intermediate in this catalytic system which is finally converted to azoarene (**P**) by two probable pathways. In path A, nitroso-arene converted to amino-arene (**N**) by similar hydride transfer via hydroxyamino-arene (**M**) formation. Further, reaction between nitroso- and amino-arene leads to the formation of azoarene by removal of water. In path B, azoxy-arene (**O**) is possible to form by the reaction between nitroso- and hydroxyamino-arene. In the subsequent step, azoxy-arene is likely to be converted to azoarene by simple hydride transfer with eliminating water. In this entire heterogeneous catalysis, formation of AuNPs-H species under UV light is probably faster than visible light which clearly portrayed by product formation in Table 1.

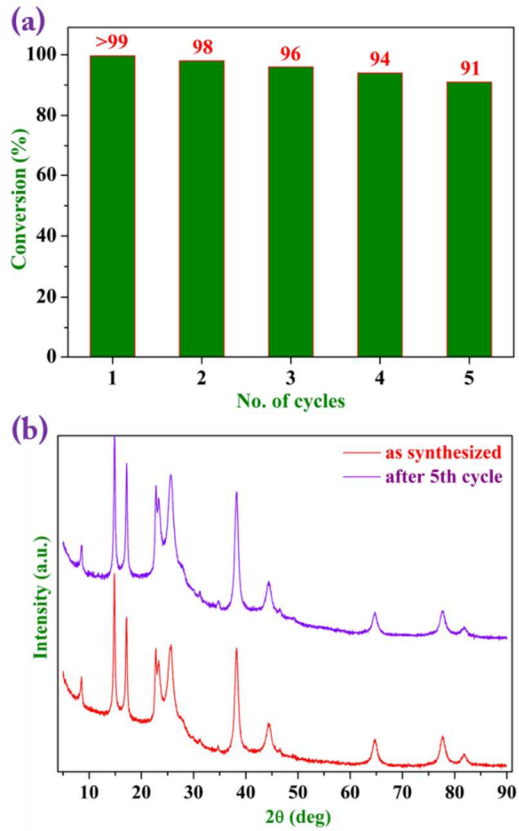

Figure 5. (a) Reusability of **Au@OC1^{R}** (conversions are based on ^{1}H NMR analysis of the crude product), (b) PXRD of recycled **Au@OC1^{R}** after 5th cycles.

For practical and industrial application of any heterogeneous catalyst, reusability is the crucial subject which makes it more beneficial over its homogeneous counterpart. Unfortunately, during catalytic reactions such small metal nanoparticles (MNPs) lose their catalytic activity because of aggregation owing to their high surface energy. Therefore, to address this key issue, the same model catalytic system was tested (reduction of 1-chloro-4-nitrobenzene) up to five consecutive cycles using **Au@OC1^{R}** as catalyst. As portrayed in the Figure 5a, a minor change in catalytic activity was observed after several cycles of reuse of the catalyst (Figure S40). PXRD analysis of **Au@OC1^{R}** was carried out after 5th cycle, which shows no significant change as compared with as-synthesized material (Figure 5b). Moreover, TEM images of the recovered material reveal same size distribution pattern with no alteration in morphology (Figures S39a, b) after the catalytic cycles. Moreover, XPS and UV-Vis spectra show a clear proof of its oxidation state (0) and characteristic absorption band with no alteration (Figures S39c, d) after catalysis. These outcomes further approve that the finely dispersed AuNPs are strongly attached to the porous architecture of organic cage and stable enough for several cycles in presence of UV light.

CONCLUSIONS

In summary, we have designed and synthesized a shape-obstinate organic molecular cage utilizing dynamic covalent chemistry. The organic cage has large interior pocket and stable aromatic backbone with cyclic thioether and vicinal diamine moieties to foster the control synthesis of AuNPs. The strong interaction between Au^{3+} with the thioether and vicinal diamine moieties of the cage is a principal factor during nucleation of the AuNPs while aromatic walls protect the newly blossomed NPs from agglomeration. The present outcomes establish the discrete organic cage compound as a novel platform for the size controlled synthesis of AuNPs using proper functionalization. As-synthesized cage supported gold nanoparticles are found to act as efficient heterogeneous photocatalyst. It offers a superior catalytic activity with selective photo-reduction of nitroarenes to form their corresponding azo compounds at ambient temperature in very short reaction time. The gifted features of these catalyst embrace with easy separation, wide range of functional group tolerance and high yield of the products. This facile and selective nitro reduction approach via a robust and recyclable cage supported AuNPs has numerous benefits over the known approaches for the conversion of nitroarenes to corresponding azo compounds as the traditional organic synthesis approaches give mixture of products containing azoxy-, amine and other byproducts. The newly developed composite establishes an innovative footstep for the advancement of new generation heterogeneous photocatalyst by tuning of structure and proper decoration of covalent cages with required functional groups.

EXPERIMENTAL SECTION

Materials and Methods: All the chemicals and solvents were purchased from available sources and used without further purification. The NMR spectra were recorded on a Bruker 400 MHz instrument. The chemical shifts (δ) in the ^{1}H, ^{13}C NMR spectra are accounted in ppm relative to TMS (Me_4Si) as an internal standard (0.0 ppm) in $CDCl_3$ or proton resonance resulting from incomplete deuteration of the solvents. High resolution mass spectra were recorded on a Q-TOF instrument by electrospray ionization (ESI) technique using standard spectroscopic grade solvents. IR spectra were recorded on a Bruker ALPHA FTIR spectrometer. Electronic absorption was recorded using a Perkin-Elmer LAMBDA 750 UV-visible spectrophotometer. Powder X-ray diffraction (PXRD) patterns were recorded on a Phillips PANalytical diffractometer. Scanning Electron Microscopy (SEM) was performed on a Carl-Zeiss Ultra 55 at an operating voltage of 3-20 kV. Transmission electron microscopy (TEM) was performed on a JEOL 2100F operating at 200 kV. X-ray photoelectron spectroscopy (XPS) was carried out on an Axis ultra-instrument. Inductively coupled plasma mass spectrometry (ICP-MS) was carried out on a Thermo-iCAP 6000 series instrument. A Philips made 60W lamp was used for UV radiation (254 and 365 nm) and visible light source was a Philips 60W LED lamp (400-700 nm) with white light. Analab μ-ThermoCal10 instrument was used for melting point range determination.

Synthesis of P1: Compound **P1** was prepared according to the literature procedure.[29a] ^{1}H NMR ($CDCl_3$, 400 MHz): δ 9.89 (s, 1H), 7.77 (d, 2H), 7.44 (d, 2H), 7.31–7.26 (m, 4H), 7.20-7.16 (m, 4H). ^{13}C NMR ($CDCl_3$, 100 MHz): δ 190.1, 150.6, 141.6, 132.7, 131.7, 130.7, 128.9, 127.4, 126.1, 125.4, 117.1. ESI-HRMS ($CHCl_3$-CH_3CN): m/z for $C_{19}H_{13}NOS$: $[M+H]^+$ 304.0775 (calcd 304.0796). FTIR (cm^{-1}) ν: 1686 (CH=O), 1580, 1463, 1281, 1222, 1167, 1112, 816, 730, 637, 533.

Synthesis of P2: Compound **P1** (1 g, 3.3 mmol) was dissolved in 60 mL of dichloromethane (DCM) in a 100 mL round bottom flask at room temperature. 1.3 g of NBS (7.25 mmol, 2.2 equv.) was added to it portion wise and refluxed with stirring for 12 h. The reaction was cooled to room temperature and washed with water several times. The combined organic phase was dried with anhydrous Na_2SO_4. The filtered organic solvent was dried over reduced pressure and the residue was purified by the column chromatography using silica gel and dichloromethane to obtain white compound **P2**. Isolated yield: 75.4% (1148 mg, 2.49 mmol). Melting point range: (143-145 ^{0}C); ^{1}H NMR ($CDCl_3$, 400 MHz): δ 9.87 (s, 1H), 8.01 (d, 2H), 7.77 (d, 2H), 7.62 (d, 2H), 7.53 (s, 2H), 7.39 (d, 2H). ^{13}C NMR ($CDCl_3$, 100 MHz): δ 191.3, 150.5, 141.5, 138.9, 136.1, 133.0, 132.0, 130.3, 127.9, 125.7, 117.4. ESI-HRMS ($CHCl_3$-CH_3CN): m/z for $C_{19}H_{11}NOSBr_2$: $[M+H]^+$ 461.8993 (calcd 461.8986). FTIR (cm^{-1}) ν: 1686 (CH=O), 1573, 1457, 1278, 1215, 1160, 1104, 829, 739, 691, 643, 522.

Synthesis of P3: In a 250 mL double-neck round-bottom flask, 2 g (4.34 mmol) of **P2** and 1.95 g (13 mmol) of 4-

formylphenylboronic acid (**3**) were taken in 100 mL THF and into that 20 mL aqueous solution of 2.4 g (17.36 mmol) K_2CO_3 was added. The resulting mixture was stirred under nitrogen atmosphere at room temperature for 10 minutes followed by addition of 250 mg (5 Mol%) of $Pd(PPh_3)_4$ and heated to 70°C for 48h. After completion of the reaction THF was removed and the crude part was extracted with dichloromethane (100 mL × 3). Organic part was then dried over anhydrous Na_2SO_4 under reduced pressure to obtain crude solid. The crude solid was purified by silica gel column chromatography in dichloromethane/hexane mixture to get yellow solid powder. Isolated yield: 80% (1.78 g, 3.48 mmol). Melting point range: (163-165 °C); ^{1}H NMR ($CDCl_3$, 400MHz): δ 9.87 (s, 1H), 9.77 (s, 2H), 8.15 (d, 2H), 8.01 (d, 4H), 7.93 (d, 2H), 7.77 (d, 4H), 7.59 (d, 2H), 7.51 (s, 2H), 7.35 (d, 2H). ^{13}C NMR (100 MHz, $CDCl_3$): δ 191.2, 190.4, 150.4, 148.1, 141.3, 139.0, 137.0, 135.6, 134.1, 132.8, 130.4, 128.0, 126.5, 125.1, 122.0, 117.6. ESI-HRMS ($CHCl_3$-CH_3CN): m/z for $C_{33}H_{21}NO_3S$: $[M+H]^+$ 512.1327 (calcd 512.1320). FTIR (cm^{-1}) ν: 1692 (CH=O), 1594, 1463, 1298, 1208, 1167, 829, 739, 691, 526, 471.

Synthesis of OC1: In a 250 mL round bottom flask 60 mL $CHCl_3$ solution of diamine **4** (33.51 mg, 0.293 mmol) was added slowly dropwise to a stirring solution of aldehyde **P3** (100 mg, 0.195 mmol) dissolved in 120 mL $CHCl_3$. The resulting reaction mixture was stirred at room temperature (298K) for 48 h. After completion of the reaction solvent was removed and the obtained yellow solid was washed with CH_3OH several times. Isolated yield: 92% (113 mg, 0.089 mmol). Melting point range: (182-184 °C); ^{1}H NMR ($CDCl_3$, 400MHz): δ 8.87 (s, 2H), 7.78 (s, 4H), 8.15 (d, 4H), 8.01 (d, 8H), 7.93 (d, 4H), 7.77 (d, 8H), 7.60 (d, 4H), 7.52 (s, 4H), 7.36 (d, 4H), 3.37 (d, 6H), 2.03-1.78 (m, 24H). ^{13}C NMR (100 MHz, $CDCl_3$): δ 162.2, 160.5, 150.1, 148.0, 141.1, 139.1, 137.0, 135.6, 134.2, 132.9, 130.3, 128.1, 126.4, 125.2, 122.2, 117.5, 74.2, 33.8, 25.5. ESI-HRMS ($CHCl_3$-CH_3CN): m/z for $C_{84}H_{72}N_8S_2$: $[M+H]^+$ 1257.5377 (calcd 1257.5400), $[M+2H]^{2+}$ 629.2769 (calcd 629.2739). FTIR (cm^{-1}) ν: 3431, 2869, 2800, 1639 (CH=N), 1567, 1421, 1332, 1257, 1015, 884, 671, 553.

Synthesis of OC1^R: In a 250 mL round bottom flask 100 mg (0.08 mmol) of **OC1** was taken in 120 mL $CHCl_3$-MeOH (1:1, v/v) binary solvent mixture. Into above reaction mixture, 36.3 mg (0.95 mmol) of $NaBH_4$ was added portion wise at room temperature (298K) and stirred for 48 h. After completion of the reaction, solvent was completely removed and the product was extracted in $CHCl_3$. Organic part was washed several times with water and dried over Na_2SO_4 followed by removal of solvent to get pale yellow solid. Isolated yield: 83.2% (84 mg, 0.066 mmol). Melting point range: (222-224 °C); ^{1}H NMR ($CDCl_3$, 400MHz): δ 8.06 (d, 4H), 7.97 (d, 8H), 7.85 (d, 4H), 7.72 (d, 8H), 7.59 (d, 4H), 7.51 (s, 4H), 7.35 (d, 4H), 4.09 (d, 4H), 3.84 (d, 8H), 2.35 (d, 6H), 1.36-1.07 (m, 24H). ^{13}C NMR (100 MHz, $CDCl_3$): δ 149.0, 147.7, 141.5, 139.7, 137.3, 135.7, 134.4, 133.0, 130.4, 128.4, 126.8, 125.4, 122.8, 117.3, 62.8, 51.6, 50.1, 32.1, 25.8. ESI-HRMS ($CHCl_3$-CH_3CN): m/z for $C_{84}H_{84}N_8S_2$: $[M+H]^+$ 1269.6366 (calcd 1269.6339). FTIR (cm^{-1}) ν: 3296, 2887, 2807, 1556, 1450, 1326, 1201, 1050, 864, 815, 774, 685, 629.

Synthesis of Au@OC1^R Catalyst: In a typical synthetic protocol, 20 mg (0.015 mmol) of **OC1^R** dissolved in 8 mL $CHCl_3$ (yellow colored) was treated with 4 mL CH_3OH solution of 66.94 mg (0.22 mmol) of $AuCl_3$ (yellow colored) and stirred for 1 h at 298K. Into this reaction mixture (brown colored), 2 mL methanolic solution of $NaBH_4$ (33.44 mg, 0.88 mmol) was added dropwise at 298K and stirred for 1h (black colored). After this said time, the solution was centrifuged to precipitate down. The product was washed several times with methanol and THF followed by drying under vacuum for overnight to obtain **Au@OC1^R** as a black solid powder.

Sample Preparation for ICP-MS Analysis: In a typical stock solution preparation, 4.63 mg of **Au@OC1^R** was added to a 10 mL concentrated nitric acid and stirred for overnight at room temperature. After complete dissolution of the catalyst, the solution was filtered to remove any undissolved materials. The filtrate was then diluted with deionized water to make a 100 mL aqueous stock solution. A series of standard aqueous solutions was prepared by dissolving $AuCl_3$ in deionized water. The experimental result shows~68 Wt% of Au in **Au@OC1^R**.

Sample Preparation for Solution State UV-Vis Spectroscopy: To prepare a stock solution, 5.26 mg of **Au@OC1^R** was taken in 10 mL $CHCl_3$ and stirred for 2 minutes to obtain a solution at 298K. In a quartz cuvette, 1980 µL of $CHCl_3$ and 20 µL of stock solution was added to get a 2 mL of solution. This solution was used for UV-Vis experiment.

General Experimental Procedure for Reduction of Nitroarenes: Typical procedure for the reduction of 1-chloro-4-nitrobenzene with **Au@OC1^R**: In a flame dried 25 mL quartz tube, 1 g (6.35 mmol) of 1-chloro-4-nitrobenzene, 50.8 mg (1.27 mmol) of NaOH and 9.12 mg (0.032 mmol, 0.5 mol% of Au) of **Au@OC1^R** were taken in 15 mL dry 2-propanol. The resulting reaction mixture was degassed and stirred under nitrogen atmosphere for 2 h under UV light. After completion, reaction mixture was filtered to separate the solid catalyst. The solid catalyst was washed with water and ethyl acetate properly and dry it in vacuum for next cycle practice. Then the filtrate was extracted with ethyl acetate (100 mL × 3). Organic part was washed with water and dried over anhydrous Na_2SO_4 followed by complete removal of solvent. The resulting crude mass was purified by silica gel column chromatography in petroleum ether/ethyl acetate (9:1, v/v) to afford pure *E*-1,2-bis(4-chlorophenyl)diazene as orange crystalline solid.

94% yield (1.51 g); orange solid; mp 186-188 °C. ^{1}H NMR ($CDCl_3$, 400MHz): δ 7.86 (d, 4H), 7.49 (d, 4H). ^{13}C NMR (100 MHz, $CDCl_3$): δ 150.9, 137.3, 129.5, 124.3. The physical data were identical in all respect to those of previously reported data.[29b]

***E*-1,2-bis(3-chlorophenyl)diazene:** 92% yield (1.47 g); orange solid; mp 99-101 °C. ^{1}H NMR ($CDCl_3$, 400MHz): δ 7.90-7.87 (m, 2H), 7.85-7.82 (m, 2H), 7.49-7.45 (m, 4H). ^{13}C NMR (100 MHz, $CDCl_3$): δ 153.1, 139.43, 131.4, 130.3, 122.7, 121.8. The physical data were identical in all respect to those previously reported.[29d]

***E*-1,2-bis(2-chlorophenyl)diazene:** 89% yield (1.43 g); red orange solid; mp 138-140 °C. ^{1}H NMR ($CDCl_3$, 400MHz): δ 7.78-7.76 (m, 2H), 7.56-7.54 (m, 2H), 7.40-7.32 (m, 4H). ^{13}C NMR (100 MHz, $CDCl_3$): δ 148.3, 135.8, 132.2, 130.5, 127.2, 118.3.[29b]

***E*-1,2-bis(4-fluorophenyl)diazene:** 91% yield (1.41 g); a yellow-orange solid; mp 100-102 °C. ^{1}H NMR ($CDCl_3$, 400MHz): δ 7.17-7.22 (m, 4H), 7.89-7.95 (m, 4H). ^{13}C NMR (100 MHz, $CDCl_3$): δ 165.7, 148.9, 124.2, 116.2.[29e]

***E*-1,2-bis(4-bromophenyl)diazene:** 93% yield (1.57 g); deep orange solid; mp 205-207 °C. ^{1}H NMR ($CDCl_3$, 400MHz): δ 7.79 (d, 4H), 7.65 (d, 4H). ^{13}C NMR (100 MHz, $CDCl_3$): δ 151.3, 132.5, 125.9, 124.5.[29b].

***E*-1,2-bis(4-iodophenyl)diazene:** 90% yield (1.57 g); a brownish-orange solid; mp 214-216 °C. ^{1}H NMR ($CDCl_3$, 400MHz): δ 7.90 (d, 4H), 7.66 (d, 4H). ^{13}C NMR (100 MHz, $CDCl_3$): δ 151.6, 138.3, 124.4, 97.75.[29c].

***E*-1,2-bisphenyldiazene:** 92% yield (1.36 g); deep orange solid; mp 65-67 °C. ^{1}H NMR ($CDCl_3$, 400MHz): δ 7.91 (d, 4H), 7.51-7.45 (m, 6H). ^{13}C NMR (100 MHz, $CDCl_3$): δ 152.8, 131.3, 129.3, 122.8.[29b]

***E*-1,2-bis(4-methylphenyl)diazene:** 91% yield (1.40 g); a red orange solid; mp 144-146 °C. ^{1}H NMR ($CDCl_3$, 400MHz): δ 7.81 (d, 4H), 7.31 (d, 4H), 2.44 (s, 6H). ^{13}C NMR (100 MHz, $CDCl_3$): δ 150.9, 141.2, 129.9, 122.4, 21.5.[29b]

***E*-1,2-bis(3-methylphenyl)diazene:** 88% yield (1.35 g); deep orange solid; mp 51-53 °C. ^{1}H NMR ($CDCl_3$, 400MHz): δ 7.74-7.71 (m, 4H), 7.40-7.38 (m, 2H), 7.30-7.27 (m, 2H), 2.47 (s, 6H). ^{13}C NMR (100 MHz, $CDCl_3$): δ 152.9, 139.1, 131.5, 129.3, 123.4, 120.4, 21.4.[29b]

***E*-1,2-bis(2-methylphenyl)diazene:** 85% yield (1.31 g); orange solid; mp 53-55 °C. ^{1}H NMR ($CDCl_3$, 400MHz): δ 7.62-7.60 (m, 2H), 7.35-7.32 (m, 4H), 7.27-7.25 (m, 2H), 2.75 (s, 6H). ^{13}C NMR (100 MHz, $CDCl_3$): δ 151.3, 138.2, 131.4, 130.4, 126.5, 115.9, 17.7.[29b]

***E*-1,2-bis(4-methoxylphenyl)diazene:** 90% yield (1.43 g); orange solid; mp 150-152 °C. ^{1}H NMR ($CDCl_3$, 400MHz): δ 7.81 (d, 4H), 7.00 (d, 4H), 3.91 (s, 6H). ^{13}C NMR (100 MHz, $CDCl_3$): δ 161.7, 147.1, 124.2, 114.2, 55.8.[29b]

***E*-1,2-bis(4-hydroxyphenyl)diazene:** 87% yield (1.34 g); pale orange solid; mp 174-176 °C. ^{1}H NMR (CD_3OD, 400MHz): δ 7.97 (d, 4H), 6.50 (d, 4H). ^{13}C NMR (100 MHz, CD_3OD): δ 161.3, 147.5, 125.4, 116.7.[15d]

***E*-1,2-bis(4-cyanophenyl)diazene:** 88% yield (1.38 g); red orange solid; mp 235-237 °C. ^{1}H NMR ($CDCl_3$, 400MHz): δ 8.05 (d, 4H), 7.86 (d, 4H). ^{13}C NMR (100 MHz, $CDCl_3$): δ 154.1, 133.5, 123.7, 118.2, 115.3.[29b]

***E*-1,2-bis(4-acetophenyl)diazene:** 87% yield (1.40 g); pale orange solid; mp 208-210 °C. ^{1}H NMR ($CDCl_3$, 400MHz): δ 8.11 (d, 4H), 8.00 (d, 4H), 2.68 (s, 6H). ^{13}C NMR (100 MHz, $CDCl_3$): δ 197.5, 154.5, 139.9, 129.7, 123.2, 26.9.[29b]

***E*-1,2-bis(4-methylcarboxylatephenyl)diazene:** 84% yield (1.39 g); orange solid; mp 224-226 °C. ^{1}H NMR ($CDCl_3$, 400MHz): δ 8.22 (d, 4H), 8.00 (d, 4H), 3.99 (s, 6H). ^{13}C NMR (100 MHz, $CDCl_3$): δ 166.4, 155.1, 132.5, 130.5, 123.1, 52.2.[29b]

***E*-1,2-bis([1,1'-biphenyl]-3-yl)diazene:** 83% yield (1.40 g); bright orange solid; mp 65.0-66.0 °C. ^{1}H NMR ($CDCl_3$, 400MHz): δ 8.20 (s, 2H), 7.94-7.92 (d, 2H), 7.75-7.70 (m, 6H), 7.63-7.59 (m, 2H), 7.51-7.47 (m, 4H), 7.42-7.38 (m, 2H). ^{13}C NMR (100 MHz, $CDCl_3$): δ 153.7, 142.8, 140.6, 130.2, 129.9, 129.4, 128.2, 127.7, 122.2.[15d]

***E*-1,2-bis(1,1'-naphthyl)diazene:** 80% yield (1.31 g); light orange solid; mp 188-190 °C. ^{1}H NMR ($CDCl_3$, 400MHz): δ 9.07 (d, 2H), 8.06-7.95 (d, 6H), 7.72-7.60 (d, 6H). ^{13}C NMR (100 MHz, $CDCl_3$): δ 152.8, 142.9, 138.7, 129.5, 128.7, 127.4. 124.1, 123.1.[29f]

Computational Methodology: Full geometry optimizations were performed using Gaussian 09 package.[30] The hybrid B3LYP functional was used in all calculations as implemented in Gaussian 09 package, mixing the exact Hartree-Fock-type exchange with Becke's expression for the exchange functional[31] that was proposed by Lee-Yang-Parr for the correlation contribution.[32] The 6-31G basis set was used for all calculations. Frequency calculations were carried on the optimized structures that confirmed the absence of any imaginary frequencies.

ASSOCIATED CONTENT

Syntheses and characterization data (NMR, FTIR, ESI-MS, TEM, SEM, PXRD). This material is available free of charge *via* the Internet at http://pubs.acs.org.

AUTHOR INFORMATION

Corresponding Author

psm@iisc.ac.in.

Notes

The authors declare no competing financial interest.

ACKNOWLEDGMENT

P. S. M. is grateful to SERB-New Delhi (India) for financial support. B. M. acknowledges the CSIR, New Delhi for the research fellowship. We are thankful to Mr. Jayanta Ghosh for theoretical calculations and Mr. Manoj Kumar for Powder XRD data collection.

REFERENCES

(1) (a) Naya, S.-i.; Kume, T.; Akashi, R.; Fujishima, M.; Tada, H. *J. Am. Chem. Soc.* **2018**, *140*, 1251-1254. (b) Shirai, K.; Fazio, G.; Sugimoto, T.; Selli, D.; Ferraro, L.; Watanabe, K.; Haruta, M.; Ohtani, B.; Kurata, H.; Di Valentin, C.; Matsumoto, Y. *J. Am. Chem. Soc.* **2018**, *140*, 1415-1422. (c) Raza, F.; Yim, D.; Park, J. H.; Kim, H.-I.; Jeon, S.-J.; Kim, J.-H. *J. Am. Chem. Soc.* **2017**, *139*, 14767-14774. (d) Tanaka, A.; Hashimoto, K.; Kominami, H. *J. Am. Chem. Soc.* **2014**, *136*, 586-589. (e) Valenti, M.; Jonsson, M.;

Biskos, G.; Schmidt-Ott, A.; Smith, W. *J. Mater. Chem. A* **2016**, *4*, 17891-17912.

(2) (a) Naya, S.-i.; Inoue, A.; Tada, H. *J. Am. Chem. Soc.* **2010**, *132*, 6292-6293. (b) Naya, S.-i.; Teranishi, M.; Isobe, T.; Tada, H. *Chem. Commun.* **2010**, *46*, 815-817. (c) Li, H.; Qin, F.; Yang, Z.; Cui, X.; Wang, J.; Zhang, L. *J. Am. Chem. Soc.* **2017**, *139*, 3513-3521.

(3) (a) Kamat, P. V. *J. Phys. Chem. B* **2002**, *106*, 7729-7744. (b) Prodan, E.; Radloff, C.; Halas, N. J.; Nordlander, P. *Science* **2003**, *302*, 419-422. (b) Mulvaney, P. *Langmuir* **1996**, *12*, 788-800. (c) Eustis, S.; El-Sayed, M. A. *Chem. Soc. Rev.* **2006**, *35*, 209-217. (d) Zhu, H.; Chen, X.; Zheng, Z.; Ke, X.; Jaatinen, E.; Zhao, J.; Guo, C.; Xie, T.; Wang, D. *Chem. Commun.* **2009**, 7524-7526. (e) Bhawawet, N.; Essner, J. B.; Atwood, J. L.; Baker, G. A. *Chem. Commun.* **2018**, *54*, 7523-7526.

(4) (a) Tsukamoto, D.; Shiraishi, Y.; Sugano, Y.; Ichikawa, S.; Tanaka, S.; Hirai, T. *J. Am. Chem. Soc.* **2012**, *134*, 6309-6315. (b) Tanaka, A.; Hashimoto, K.; Kominami, H. *J. Am. Chem. Soc.* **2012**, *134*, 14526-14533. (c) Li, B.; Gu, T.; Ming, T.; Wang, J.; Wang, P.; Wang, J.; Yu, J. C. *ACS nano* **2014**, *8*, 8152-8162.

(5) (a) Kelly, K. L.; Coronado, E.; Zhao, L. L.; Schatz, G. C. *J. Phys. Chem. B* **2003**, *107*, 668-677. (b) Balamurugan, B.; Maruyama, T. *Appl. Phys. Lett.* **2005**, *87*, 143105.

(6) Koyama, D.; Dale, H. J.; Orr-Ewing, A. J. *J. Am. Chem. Soc.* **2018**, *140*, 1285–1293.

(7) (a) Zhu, H.; Ke, X.; Yang, X.; Sarina, S.; Liu, H. *Angew. Chem.* **2010**, *122*, 9851-9855. (b) Linic, S.; Aslam, U.; Boerigter, C.; Morabito, M. *Nat. Mater.* **2015**, *14*, 567. (c) Hao, C.-H.; Guo, X.-N.; Pan, Y.-T.; Chen, S.; Jiao, Z.-F.; Yang, H.; Guo, X.-Y. *J. Am. Chem. Soc.* **2016**, *138*, 9361-9364.

(8) Qian, K.; Sweeny, B. C.; Johnston-Peck, A. C.; Niu, W.; Graham, J. O.; DuChene, J. S.; Qiu, J.; Wang, Y.-C.; Engelhard, M. H.; Su, D. *J. Am. Chem. Soc.* **2014**, *136*, 9842-9845.

(9) (a) Gianneschi, N. C.; Masar, M. S.; Mirkin, C. A. *Acc. Chem. Res.* **2005**, *38*, 825-837. (b) Chakrabarty, R.; Mukherjee, P. S.; Stang, P. J. *Chem. Rev.* **2011**, *111*, 6810-6918. (c) Smulders, M. M.; Jiménez, A.; Nitschke, J. R. *Angew. Chem.* **2012**, *124*, 6785-6789. (d) Sun, Q.-F.; Sato, S.; Fujita, M. *Nat. Chem.* **2012**, *4*, 330. (e) Lehn, J.-M. *Chem. Soc. Rev.* **2017**, *46*, 2378-2379. (f) Holloway, L. R.; Bogie, P. M.; Lyon, Y.; Ngai, C.; Miller, T. F.; Julian, R. R.; Hooley, R. J. *J. Am. Chem. Soc.* **2018**, *140*, 8078-8081. (g) Cao, L.; Wang, P.; Miao, X.; Dong, Y.; Wang, H.; Duan, H.; Yu, Y.; Li, X.; Stang, P. J. *J. Am. Chem. Soc.* **2018**, *140*, 7005-7011.

(10) (a) Cook, T. R.; Stang, P. J. *Chem. Rev.* **2015**, *115*, 7001-7045. (b) Lee, H.; Elumalai, P.; Singh, N.; Kim, H.; Lee, S. U.; Chi, K.-W. *J. Am. Chem. Soc.* **2015**, *137*, 4674-4677. (c) Chen, L.-J.; Chen, S.; Qin, Y.; Xu, L.; Yin, G.-Q.; Zhu, J.-L.; Zhu, F.-F.; Zheng, W.; Li, X.; Yang, H.-B. *J. Am. Chem. Soc.* **2018**, *140*, 5049-5052. (d) Wang, W.; Wang, Y.-X.; Yang, H.-B. *Chem. Soc. Rev.* **2016**, *45*, 2656-2693. (e) Wei, P.; Yan, X.; Huang, F. *Chem. Soc. Rev.* **2015**, *44*, 815-832. (f) Sun, B.; Wang, M.; Lou, Z.; Huang, M.; Xu, C.; Li, X.; Chen, L.-J.; Yu, Y.; Davis, G. L.; Xu, B. *J. Am. Chem. Soc.* **2015**, *137*, 1556-1564.

(11) (a) Cougnon, F. B.; Sanders, J. K. *Acc. Chem. Res.* **2011**, *45*, 2211-2221. (b) Jin, Y.; Voss, B. A.; Jin, A.; Long, H.; Noble, R. D.; Zhang, W. *J. Am. Chem. Soc.* **2011**, *133*, 6650-6658. (c) Acharyya, K.; Mukherjee, S.; Mukherjee, P. S. *J. Am. Chem. Soc.* **2012**, *135*, 554-557. (d) Zhang, G.; Presly, O.; White, F.; Oppel, I. M.; Mastalerz, M. *Angew. Chem., Int. Ed.* **2014**, *126*, 5226-5230. (e) Tozawa, T.; Jones, J. T.; Swamy, S. I.; Jiang, S.; Adams, D. J.; Shakespeare, S.; Clowes, R.; Bradshaw, D.; Hasell, T.; Chong, S. Y. *Nat. Mater.* **2009**, *8*, 973. (f) Mitra, T.; Jelfs, K. E.; Schmidtmann, M.; Ahmed, A.; Chong, S. Y.; Adams, D. J.; Cooper, A. I. *Nat. Chem.* **2013**, *5*, 276-281. (g) Jin, Y.; Yu, C.; Denman, R. J.; Zhang, W. *Chem. Soc. Rev.* **2013**, *42*, 6634-6654.

(12) (a) Vajda, S.; Pellin, M. J.; Greeley, J. P.; Marshall, C. L.; Curtiss, L. A.; Ballentine, G. A.; Elam, J. W.; Catillon-Mucherie, S.; Redfern, P. C.; Mehmood, F. *Nat. Mater.* **2009**, *8*, 213. (b) Qiao, B.; Wang, A.; Yang, X.; Allard, L. F.; Jiang, Z.; Cui, Y.; Liu, J.; Li, J.; Zhang, T. *Nat. Chem.* **2011**, *3*, 634. (c) Li, Z.; Liu, J.; Xia, C.; Li, F. *ACS Catal.* **2013**, *3*, 2440-2448. (d) Kibata, T.; Mitsudome, T.; Mizugaki, T.; Jitsukawa, K.; Kaneda, K. *Chem. Commun.* **2013**, *49*, 167-169. (e) Leifert, A.; Pan-Bartnek, Y.; Simon, U.; Jahnen-Dechent, W. *Nanoscale* **2013**, *5*, 6224-6242. (f) Abad, A.; Concepción, P.; Corma, A.; García, H. *Angew. Chem., Int. Ed.* **2005**, *44*, 4066-4069.

(13) (a) Crooks, R. M.; Zhao, M.; Sun, L.; Chechik, V.; Yeung, L. K. *Acc. Chem. Res.* **2001**, *34*, 181-190. (b) Scott, R. W.; Sivadinarayana, C.; Wilson, O. M.; Yan, Z.; Goodman, D. W.; Crooks, R. M. *J. Am. Chem. Soc.* **2005**, *127*, 1380-1381. (c) Balogh, L.; Tomalia, D. A. *J. Am. Chem. Soc.* **1998**, *120*, 7355-7356. (d) Zheng, J.; Petty, J. T.; Dickson, R. M. *J. Am. Chem. Soc.* **2003**, *125*, 7780-7781. (e) Zheng, J.; Dickson, R. M. *J. Am. Chem. Soc.* **2002**, *124*, 13982-13983. (f) White, R. J.; Luque, R.; Budarin, V. L.; Clark, J. H.; Macquarrie, D. J. *Chem. Soc. Rev.* **2009**, *38*, 481-494.

(14) (a) Farmer, J. A.; Campbell, C. T. *Science* **2010**, *329*, 933-936. (b) Campbell, C. T. *Acc. Chem. Res.* **2013**, *46*, 1712-1719. (c) Prieto, G.; Zečević, J.; Friedrich, H.; De Jong, K. P.; De Jongh, P. E. *Nat. Mater.* **2013**, *12*, 34. (d) Nasir Baig, R. B.; Varma, R. S. *ACS Sustainable Chem. Eng.* **2013**, *1*, 805-809. (e) Su, F.-Z.; He, L.; Ni, J.; Cao, Y.; He, H.-Y.; Fan, K.-N. *Chem. Commun.* **2008**, 3531-3533.

(15) (a) Aijaz, A.; Karkamkar, A.; Choi, Y. J.; Tsumori, N.; Rönnebro, E.; Autrey, T.; Shioyama, H.; Xu, Q. *J. Am. Chem. Soc.* **2012**, *134*, 13926-13929. (b) Jiang, H. L.; Lin, Q. P.; Akita, T.; Liu, B.; Ohashi, H.; Oji, H.; Honma, T.; Takei, T.; Haruta, M.; Xu, Q. *Chem.- Eur J* **2011**, *17*, 78-81. (c) Lu, G.; Li, S.; Guo, Z.; Farha, O. K.; Hauser, B. G.; Qi, X.; Wang, Y.; Wang, X.; Han, S.; Liu, X. *Nat. Chem.* **2012**, *4*, 310. (d) Gole, B.; Sanyal, U.; Mukherjee, P. S. *Chem. Commun.* **2015**, *51*, 4872-4875. (e) Hu, P.; Zhuang, J.; Chou, L.-Y.; Lee, H. K.; Ling, X. Y.; Chuang, Y.-C.; Tsung, C.-K. *J. Am. Chem. Soc.* **2014**, *136*, 10561-10564. (f) Meilikhov, M.; Yusenko, K.; Esken, D.; Turner, S.; Van Tendeloo, G.; Fischer, R. A. *Eur. J. Inorg. Chem.* **2010**, 3701-3714.

(16) (a) Li, L.; Zhao, H.; Wang, J.; Wang, R. *ACS nano* **2014**, *8*, 5352-5364. (b) Zhang, Q.; Yang, Y.; Zhang, S. *Chem.- Eur. J* **2013**, *19*, 10024-10029. (c) Zhou, Y.; Xiang, Z.; Cao, D.; Liu, C.-J. *Chem. Commun.* **2013**, *49*, 5633-5635. (d) Pachfule, P.; Panda, M. K.; Kandambeth, S.; Shivaprasad, S.; Díaz, D. D.; Banerjee, R. *J. Mater. Chem. A* **2014**, *2*, 7944-7952 (e) Pachfule, P.; Kandambeth, S.; Díaz, D. D.; Banerjee, R. *Chem. Commun.* **2014**, *50*, 3169-3172. (f) Lu, S.; Hu, Y.; Wan, S.; McCaffrey, R.; Jin, Y.; Gu, H.; Zhang, W. *J. Am. Chem. Soc.* **2017**, *139*, 17082-17088.

(17) (a) McCaffrey, R.; Long, H.; Jin, Y.; Sanders, A.; Park, W.; Zhang, W., *J. Am. Chem. Soc.* **2014**, *136*, 1782-1785. (b) Sun, J.-K.; Zhan, W.-W.; Akita, T.; Xu, Q., *J. Am. Chem. Soc.* **2015**, *137*, 7063-7066. (c) Mondal, B.; Acharyya, K.; Howlader, P.; Mukherjee, P. S., *J. Am. Chem. Soc.* **2016**, *138*, 1709-1716. (d) Qiu, L.; McCaffrey, R.; Jin, Y.; Gong, Y.; Hu, Y.; Sun, H.; Park, W.; Zhang, W., *Chem. Sci.* **2018**, *9*, 676-680. (e) Zhang, Y.; Xiong, Y.; Ge, J.; Lin, R.; Chen, C.; Peng, Q.; Wang, D.; Li, Y., *Chem. Commun.* **2018**, *54*, 2796-2799. (f) Yang, X.; Sun, J.-K.; Kitta, M.; Pang, H.; Xu, Q. *Nature Catalysis* **2018**, *1*, 214-220.

(18) Hunger, K., *Industrial dyes: chemistry, properties, applications*. John Wiley & Sons: 2007.

(19) Chudgar, R. J. Kirk-Othmer Encyclopedia of Chemical Technology, Vol. 3, 4th ed., Wiley, New York, 1992.

(20) (a) Hunger, K., *Industrial dyes: Chemistry, properties, applications.* 2003, 625-641. (b) Anderson, R.; Nickless, G. *Analyst* **1967**, *92*, 207-238. (c) ASHUTOSH; Pandey, N.;

Mehrotra, J. *Colourage* **1979**, *26*, 25-25. (d) Sandborn, W. J. *Am. J. Gastroenterol.* **2002**, *97*, 2939-2941.

(21) Ma, H.; Li, W.; Wang, J.; Xiao, G.; Gong, Y.; Qi, C.; Feng, Y.; Li, X.; Bao, Z.; Cao, W. *Tetrahedron* **2012**, *68*, 8358-8366.

(22) (a) Dabbagh, H. A.; Teimouri, A.; Chermahini, A. N. *Dyes and pigments* **2007**, *73*, 239-244. (b) Barbero, M.; Cadamuro, S.; Dughera, S.; Giaveno, C. *Eur. J. Org. Chem.* **2006**, 4884-4890.

(23) Liu, Z.; Jiang, M. *J. Mater. Chem.* **2007**, *17*, 4249-4254.

(24) (a) Merino, E. *Chem. Soc. Rev.* **2011**, *40*, 3835-3853. (b) Dutta, B.; Biswas, S.; Sharma, V.; Savage, N. O.; Alpay, S. P.; Suib, S. L. *Angew. Chem., Int. Ed.* **2016**, *128*, 2211-2215. (c) Liu, X.; Li, H. Q.; Ye, S.; Liu, Y. M.; He, H. Y.; Cao, Y. *Angew. Chem., Int. Ed.* **2014**, *53*, 7624-7628. (d) Peiris, S.; McMurtrie, J.; Zhu, H.-Y. *Catal. Sci. Technol.* **2016**, *6*, 320-338. (e) Xu, Q.; Liu, X.; Chen, J.; Li, R.; Li, X. *J Mol Catal A* **2006**, *260*, 299-305.

(25) Combita, D.; Concepción, P.; Corma, A. *J. Catal.* **2014**, *311*, 339-349.

(26) (a) Grirrane, A.; Corma, A.; García, H. *Science* **2008**, *322*, 1661-1664. (b) Corma, A.; Concepción, P.; Serna, P. *Angew. Chem., Int. Ed.* **2007**, *119*, 7404-7407.

(27) (a) Corma, A.; Serna, P. *Science* **2006**, *313*, 332-334. (b) Grirrane, A.; Corma, A.; Garcia, H. *Nat. Protoc.* **2010**, *5*, 429.

(28) (a) Fagnoni, M.; Dondi, D.; Ravelli, D.; Albini, A. *Chem. Rev.* **2007**, *107*, 2725-2756. (b) Chen, X.; Mao, S. S. *Chem. Rev.* **2007**, *107*, 2891-2959.

(29) (a) Xue, P.; Ding, J.; Chen, P.; Wang, P.; Yao, B.; Sun, J.; Sun, J.; Lu, R. *J. Mater. Chem. C* **2016**, *4*, 5275-5280. (b) Sakai, N.; Asama, S.; Anai, S.; Konakahara, T. *Tetrahedron* **2014**, *70*, 2027-2033. (c) Zhao, R.; Tan, C.; Xie, Y.; Gao, C.; Liu, H.; Jiang, Y. *Tetrahedron Lett.* **2011**, *52*, 3805-3809. (d) Liu, X.; Ye, S.; Li, H.-Q.; Liu, Y.-M.; Cao, Y.; Fan, K.-N. *Catal. Sci. Technol.* **2013**, *3*, 3200-3206. (e) Pothula, K.; Tang, L.; Zha, Z.; Wang, Z. *RSC Adv.* **2015**, *5*, 83144-83148. (f) Seth, K.; Roy, S. R.; Kumar, A.; Chakraborti, A. K. *Catal. Sci. Technol.* **2016**, *6*, 2892-2896.

(30) Gaussian 09, Revision A.02, M. J. Frisch, G. W. Trucks, H. B. Schlegel, G. E. Scuseria, M. A. Robb, J. R. Cheeseman, G. Scalmani, V. Barone, B. Mennucci, G. A. Petersson, H. Nakatsuji, M. Caricato, X. Li, H. P. Hratchian, A. F. Izmaylov, J. Bloino, G. Zheng, J. L. Sonnenberg, M. Hada, M. Ehara, K. Toyota, R. Fukuda, J. Hasegawa, M. Ishida, T. Nakajima, Y. Honda, O. Kitao, H. Nakai, T. Vreven, J. A. Montgomery, Jr., J. E. Peralta, F. Ogliaro, M. Bearpark, J. J. Heyd, E. Brothers, K. N. Kudin, V. N. Staroverov, R. Kobayashi, J. Normand, K. Raghavachari, A. Rendell, J. C. Burant, S. S. Iyengar, J. Tomasi, M. Cossi, N. Rega, J. M. Millam, M. Klene, J. E. Knox, J. B. Cross, V. Bakken, C. Adamo, J. Jaramillo, R. Gomperts, R. E. Stratmann, O. Yazyev, A. J. Austin, R. Cammi, C. Pomelli, J. W. Ochterski, R. L. Martin, K. Morokuma, V. G. Zakrzewski, G. A. Voth, P. Salvador, J. J. Dannenberg, S. Dapprich, A. D. Daniels, O. Farkas, J. B. Foresman, J. V. Ortiz, J. Cioslowski, and D. J. Fox, Gaussian, Inc., Wallingford CT, 2009.

(31) Becke, A. D. *Phys. Rev. A* **1988**, *38*, 3098.

(32) Lee, C.; Yang, W.; Parr, R. G. *Phys. Rev. B* **1988**, *37*, 785.

Cage Encapsulated Gold Nanoparticles as Heterogeneous Photocatalyst for Facile and Selective Reduction of Nitroarenes to Azo Compounds

Bijnaneswar Mondal and Partha Sarathi Mukherjee*